Fractal generalized zone plates

Omel Mendoza-Yero,[1,*] **Mercedes Fernández-Alonso,**[1] **Gladys Mínguez-Vega,**[1] **Jesús Lancis,**[1] **Vicent Climent,**[1] **and Juan A. Monsoriu**[2]

[1]*GROC, Departament de Física, Universitat Jaume I, E12080 Castelló, Spain*
[2]*Departamento de Física Aplicada, Universidad Politécnica de Valencia,
E-46022 Valencia, Spain*
*Corresponding author: omendoza@uji.es

The construction of fractal generalized zone plates from a set of periodic diffractive optical elements with circular symmetry is proposed. This allows us, for instance, to increase the number of foci of a conventional fractal zone plate while keeping the self-similarity property within the axial irradiance. The focusing properties of these fractal diffractive optical elements for points not only along but also in the close vicinity of the optical axis are investigated. In both cases analytical expressions for the irradiance are derived. Numerical simulations of the energetic efficiency of fractal generalized zone plates under plane wave illumination are carried out. In addition, some effects on the axial irradiance caused by variations in the area of their transparent rings are shown. © 2009 Optical Society of America

OCIS codes: 050.1220, 050.1970.

1. INTRODUCTION

Fractal structures play an important role in being able to describe and understand a large number of phenomena in several areas of science and technology [1]. Within the optical community, there is a growing interest in implementing optical structures that exhibit fractal properties. Among these, it has been shown that optical fields derived from the diffraction of waves by fractal structures can originate self-similar on-axis irradiance profiles under monochromatic illumination [2,3]. This means that, within a focal energy distribution, some of its parts have the same shape as the whole irradiance profile. This phenomenon appears when we deal with a fractal zone plate (FraZP) designed on the basis of the well-known Fresnel zone plates (FZPs) [4,5]. The focusing properties of the optical elements of the former have been investigated theoretically, using the Fresnel approximation [2,3], as well as by means of an experimental implementation with liquid-crystal displays [6,7]. In practice, FraZPs have been used to produce a sequence of focused optical vortices [8] or to achieve optical images with an extended depth of field and reduced chromatic aberration under white-light illumination [9].

In this paper, the construction of fractal generalized zone plates (FraGZPs) from a set of GZPs is proposed. By GZP we mean a circularly symmetric binary pupil that is periodic in the squared radial coordinate and in which the ratio between the areas of the whole period and its transparent part is a positive integer number ε. In accordance with the above definition, a conventional FZP is a particular case of a GZP with $\varepsilon = 2$, because within a period the areas of opaque and transparent regions are equal. It should be noted that the focusing properties of these GZPs under monochromatic and femtosecond illumination were studied extensively in [10]. With the introduc-

tion of FraGZPs, the number of foci and the diffraction efficiency within certain axial intervals are increased in comparison with similar aspects of FraZPs. We find that increasing the number of foci of a FraZP could be applied, for instance, to trap and manipulate particles at different controlled levels by means of a spiral FraZP [8]. From an analytical point of view, expressions are determined for the irradiance along the optical axis or for the position and peak height of several intense foci. The self-similar property within the irradiance patterns of FraGZPs, which is derived from these results, is also shown.

On the other hand, thanks to the diffractive nature of FraZPs, they can be used in optical regions where refractive optics is not available due to the strong absorption of materials, such as those related to soft x-ray microscopy or terahertz imaging, where FZPs have been successfully applied [11,12]. To this end, it is essential to know the diffraction-limited resolution and/or the energetic efficiency of the fractal structures. In this work, a novel study of the three-dimensional light distribution of fractal structures in the vicinity of the optical axis is included. To carry out this study, an approximate analytical expression for the irradiance of circularly symmetric binary plates in the vicinity of the optical axis was achieved.

The structure of the manuscript is as follows. In Section 2, the procedure for constructing the proposed fractal structures is described, and then their on-axis focusing properties are investigated. In Section 3, the off-axis behavior as well as the energy efficiency of our plates is shown by means of some illustrated examples and particular integrals. To emphasize the main features of the fractal plates introduced here, we summarize their attributes in Section 4, and our conclusions are given in Section 5.
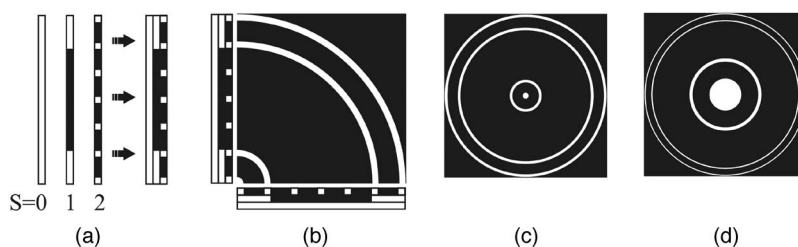
Fig. 1.   Steps for construction of a FraGZP with $N=2$ and $S=2$ from GZPs with $\varepsilon=4$. (a) geometric bars, (b) rotation process, (c) pupil in r^2, and (d) pupil in r.

2. ON-AXIS FOCUSING PROPERTIES OF FRACTAL GENERALIZED ZONE PLATES

The construction of a FraGZP from a set of GZPs is shown in Fig. 1 for $\varepsilon=4$. In accordance with the notation for FraZPs [2], $N=1,2,\ldots$ is the number of segments within the fractal structure, and $S=0,1,\ldots$ is the number of recursion times or fractal levels. In addition, the outermost ring radius of the resulting plate is denoted by a. To determine the spatial distribution of their zones, the radii in the squared radial coordinate of transparent and opaque rings of each GZP are represented by consecutive open and filled line segments, thus forming a geometric bar. All bars are placed near each other and aligned to form a column of bar lines. The amplitude transmittance in the squared radial coordinate of the binary pupil is then obtained from the rotation of the whole structure around one extreme. In this process, the open segments that coincide in position with filled ones are canceled out. After the change of variable, the remaining open segments become the transparent rings of the resulting binary pupils.

It can be shown that the period of GZPs normalized to a^2 is given by $p=\varepsilon/(\varepsilon N-(\varepsilon-1))^S$. After taking into account the dependence of p on the parameter ε, the on-axis irradiance of a FraZP [2] can be generalized and rewritten in the form

$$I_{FraGZP}(u,N,S,\varepsilon)$$
$$=I_{GZP}(u,N,S,\varepsilon)\prod_{i=1}^{S-1} \sin^2\!\left(N\frac{\varepsilon\pi u}{(\varepsilon N-(\varepsilon-1))^i}\right)\Bigg/$$
$$\sin^2\!\left(\frac{\varepsilon\pi u}{(\varepsilon N-(\varepsilon-1))^i}\right), \qquad (1)$$

where $I_{GZP}(u,N,S,\varepsilon)$ denotes the on-axis irradiance originated by a GZP, with N transparent rings and period p, that is illuminated with a monochromatic plane wave:

$$I_{GZP}(u,N,S,\varepsilon)$$
$$=4\sin^2\!\left(\frac{\pi u}{(\varepsilon N-(\varepsilon-1))^S}\right)\sin^2\!\left(M\frac{\varepsilon\pi u}{(\varepsilon N-(\varepsilon-1))^S}\right)\Bigg/$$
$$\sin^2\!\left(\frac{\varepsilon\pi u}{(\varepsilon N-(\varepsilon-1))^S}\right). \qquad (2)$$

In Eqs. (1) and (2) the term $u=a^2/(2\lambda z)$ is a normalized axial coordinate. Here, it should be pointed out that the number of transparent rings is given by M in Eq. (2) in order to prevent it from being mixed with variable N, even when in this particular case $M=N$. The slowly oscil-

lating right-hand term in Eq. (2) determines the energy content of the different foci. The trigonometric quotient allows us to derive their axial locations, given by $z_n =pa^2/(2\lambda n)$, with $n=1,2,\ldots$, and so on. An exception occurs when the equality $n=m\varepsilon$ is fulfilled, where m is also a positive integer. In this case, the focus transforms into a phase singularity where the intensity vanishes [10]. The function given by Eq. (1) also achieves maximum values at the positions $z=z_n$. The foci associated with the position are referred to as "principal foci," and the remaining ones are called "secondary foci." The peak heights of the principal foci are assessed after solving the limit of $I_{FraGZP}(u,N,S,\varepsilon)$ as z approaches z_n, the value of which is $4N^{2S}\sin^2(n\pi/\varepsilon)$.

To analyze the on-axis focusing characteristics under monochromatic illumination of FraGZPs, six irradiance curves are plotted in Fig. 2 (top and middle rows). To obtain the curves, the parameters $N=2$, $S=2,3$, $a=10^{-2}$ m, $\lambda=780$ nm and $\varepsilon=2,3$, and 4 were substituted into Eq. (1). The self-similarity property is observed from two characteristic irradiance profiles with different fractal levels. That is, the patterns with $S=3$ (top row of Fig. 2) are modulated versions of the corresponding ones in the previous stage $S=2$ but now plotted just in the middle row.

The irradiance profiles caused by the associated GZPs are shown in the bottom row of Fig. 2 (only for $S=2$), after setting $M=(\varepsilon N-(\varepsilon-1))^S/\varepsilon+(\varepsilon-1)/\varepsilon$ in Eq. (2). In this case, the peak heights of their principal foci are also determined from Eq. (2) to yield $4M^2\sin^2(n\pi/\varepsilon)$.

From the insets in the middle and bottom curves of Fig. 2 it can be noted that a FraGZP is no more than a GZP with some of its transparent rings missing. Furthermore, a FraGZP with $S=2$ may be considered to be a particular case of a lacunar FraZP [3]. However, this does not apply to the case $S=3$ or higher fractal orders

After a visual inspection of Fig. 2 it is clear that the number of foci becomes higher as the parameter ε increases. Within a characteristic irradiance profile of a FraGZP, this number is given approximately by $(\varepsilon-1)(\varepsilon +1)^{S-1}$ for an even value of the parameter ε, whereas it yields $(\varepsilon-1)\varepsilon^{S-1}$ for an odd value of it. The above expressions do not take into account irradiance peaks with relatively low heights. For instance, for FraGZPs with parameters $[\varepsilon=2, S=2]$ and $[\varepsilon=3, S=2]$, irradiance peaks with less than 6.3% and 4.2%, respectively, of the maximum peak height are not considered in the above expressions. Note that the peak heights of some secondary foci, numerically determined from Eq. (1), cannot be disregarded because they have an order of magnitude similar to that
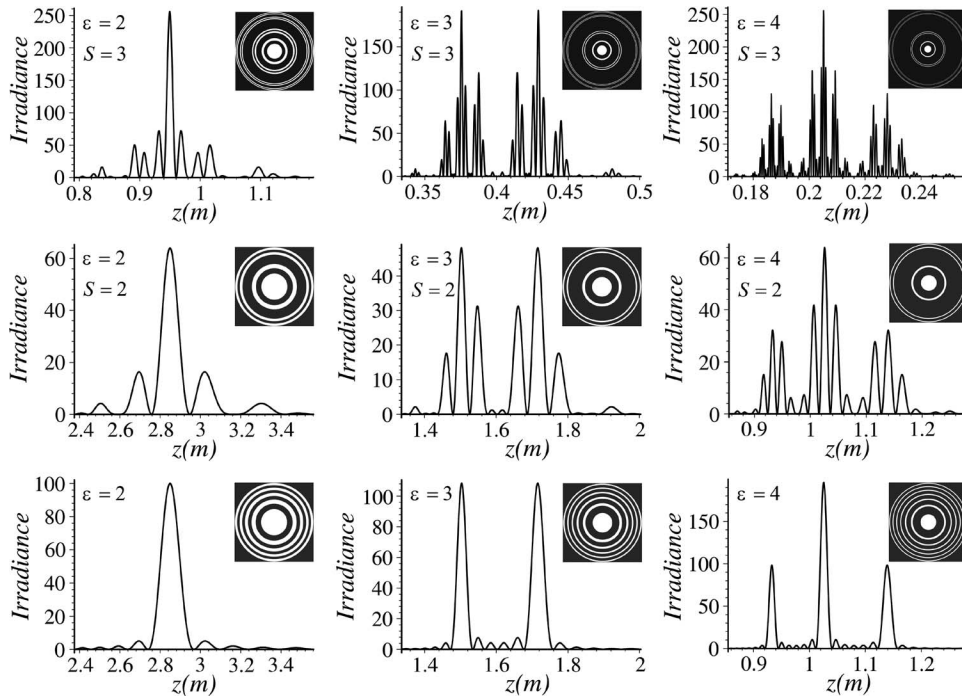
Fig. 2. Characteristic irradiance profiles of FraGZPs (top and middle rows) and GZPs (bottom row).

of the principal foci. The common foci are identified by comparing the characteristic irradiance profiles of a FraGZP and its corresponding GZP.

3. THREE-DIMENSIONAL LIGHT DISTRIBUTION AROUND THE OPTICAL AXIS

The off-axis behavior of the diffracted field cannot be studied with the above formulation. To study such behavior, an approximate analytical expression for the irradiance in terms of the first Rayleigh–Sommerfeld diffraction integral can be derived [13]. For points in the close vicinity of the optical axis it yields

$$
\begin{aligned}
I(u,R) = &\left\{ \sum_{m=1}^{M} \left[J_0\!\left(4\pi \frac{ur_{im}R}{a^2} \right) \cos\!\left(2\pi \frac{ur_{im}^2}{a^2} \right) \right. \right. \\
&\left. - J_0\!\left(4\pi \frac{ur_{om}R}{a^2} \right) \cos\!\left(2\pi \frac{ur_{om}^2}{a^2} \right) \right]\Bigg\}^2 \\
&+ \left\{ \sum_{m=1}^{M} \left[J_0\!\left(4\pi \frac{ur_{im}R}{a^2} \right) \sin\!\left(2\pi \frac{ur_{im}^2}{a^2} \right) \right. \right. \\
&\left. - J_0\!\left(4\pi \frac{ur_{om}R}{a^2} \right) \sin\!\left(2\pi \frac{ur_{om}^2}{a^2} \right) \right]\Bigg\}^2 .
\end{aligned}
\tag{3}
$$

In Eq. (3), r_{im} and r_{om} denote the inner and outer radii of the transparent rings, which are given by $r_{im} = a[p(m-1)]^{1/2}$ and $r_{om} = a\{p[m-(1-1/\varepsilon)]\}^{1/2}$, respectively, for a GZP. The radial coordinate in the output transversal plane is given by the variable R. The function $J_0(x)$ is the Bessel function of the first kind with order zero and argument x. In general, Eq. (3) can be applied to simulate the off-axis irradiance created by the diffraction of a plane wave through any binary amplitude pupils with circular

symmetry. In the case of a FraGZP, care must be taken to consider only the suffixes m corresponding to the remaining clear zones that result from the construction process (see Fig. 1). When $R = 0$, we can use Eq. (3) to plot the curves of Fig. 2.

To be consistent with the previous analysis, we focus our attention on the off-axis behavior of the irradiance caused by the pupils depicted in Fig. 2 and, more specifically, those characterized by $S = 2$ together with GZPs. Figure 3 shows the complex structure of foci near the optical axis. From the three-dimensional light distribution, one can compare the ability of FraGZPs and corresponding GZPs to concentrate the energy around the optical axis.

If we look carefully at the light distributions in Fig. 3, we can observe that the transversal widths of the principal foci are almost the same for a fractal structure and its corresponding GZP but that the axial width is reduced with the first of the two pupils. The latter effect can perhaps be seen more clearly in Fig. 2. This behavior suggests that a FraGZP could be used as a lens to enhance the resolving power of a GZP, bearing in mind that the peak height is lower when using a fractal pupil. To give a numerical example, we assessed the full width at half-maximum in the axial direction of the foci at $z = z_7$ for the pupils in Fig. 2 with $\varepsilon = 3$ and $S = 2$. In this case, the ratio between the corresponding values yields a value of 0.87.

There is currently a growing interest in the use of zone plates for microscopy, micromachining, and lithography [14,15]. Within this context, the energy efficiency of the binary pupils on any transversal plane z is determined. We evaluate the expression $E_{eff}(R_0) = 2\pi \int_0^{R_0} I(u,R)R\,dR/(\pi a^2)$, which gives us the ratio between the energy transmitted by a pinhole of radius R_0 on the output plane z and the energy of the incident plane wave within the pupil area $A = \pi a^2$. The results for the bi-
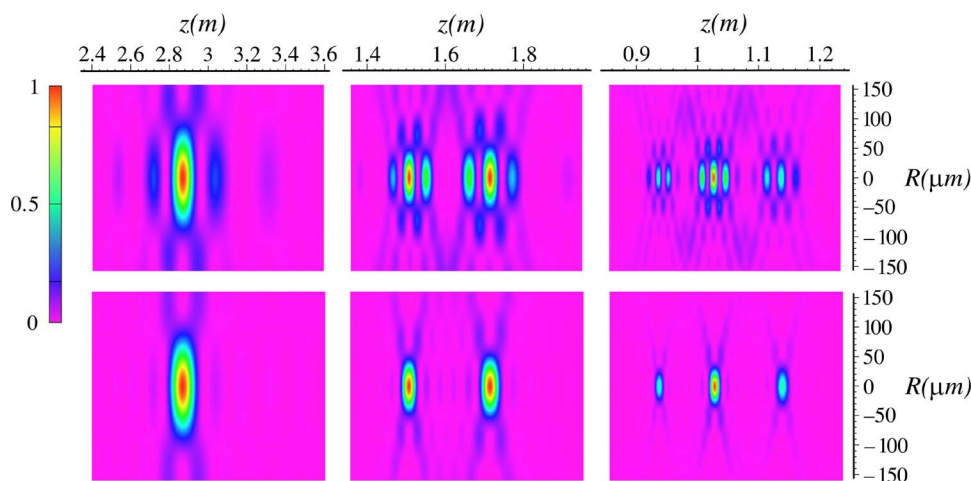
Fig. 3. (Color online) Normalized off-axis irradiance profiles of FraGZPs (top) and GZPs (bottom) given in the middle and bottom rows of Fig. 2.
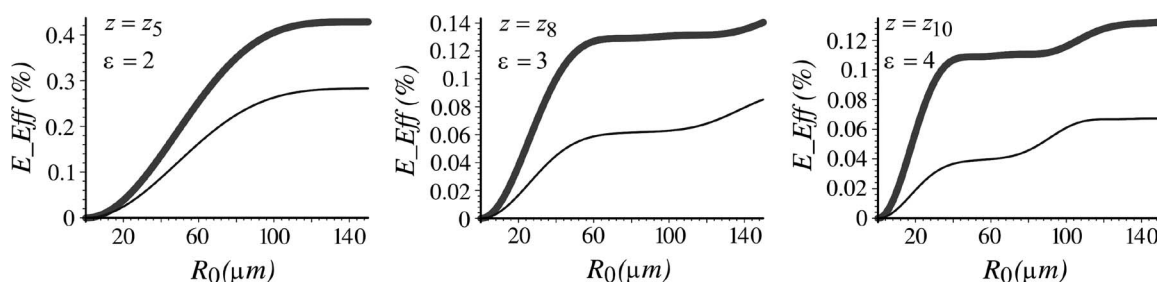

Fig. 4. Energy efficiency of FraGZPs (thin curves) and GZPs (thick curves) on the planes $z=z_5$ (for $\varepsilon=2$), $z=z_8$ (for $\varepsilon=3$), and $z=z_{10}$ (for $\varepsilon=4$). In all cases $S=2$.

nary pupils used in Fig. 3 on three principal planes $z=z_n$ are shown in Fig. 4, where the radius R_0 varies from 0 to 150 μm. Because of the absence of some rings for the foci that were compared, FraGZPs are seen to be less efficient than the corresponding GZPs. This difference is reduced as ε tends to 2 (see insets in Fig. 2).

Within characteristic irradiance profiles like those shown in Fig. 2 and 3, the energy distributed among foci along the optical axis is evaluated by calculating the integrals $E_{FraGZP}=\int_{u_{in}}^{u_{out}}I_{FraGZP}(u,N,S,\varepsilon)\mathrm{d}u$ and $E_{GZP}=\int_{u_{in}}^{u_{out}}I_{GZP}(u,N,S,\varepsilon)\mathrm{d}u$. The limits of the above integrals extends from $u_{in}=t\varepsilon/p$ to $u_{out}=(t+1)\varepsilon/p$, where a value of $t=1,2,\ldots$ denotes a given axial interval. From the analysis of the results $E_{FraGZP}=2N^S\varepsilon/p$ and $E_{GZP}=2M\varepsilon/p$, again with $M=(\varepsilon N-(\varepsilon-1))^S/\varepsilon+(\varepsilon-1)/\varepsilon$ and $p=\varepsilon/(\varepsilon N-(\varepsilon-1))^S$, it can be verified that (a) the diffraction efficiency of GZPs is better than that of FraGZPs within the whole intervals in Fig. 2 and 3, and (b) the energy along the optical axis contained within a characteristic profile increases as the parameter ε increases, due to diffraction by FraGZPs. The calculus of the energetic efficiency of binary pupils is a necessary requirement for many experiments, such as the generation of nonlinear effects, where FZPs have been successfully applied [16,17]. In this context, kinoform and multiphase level FraZPs are currently under development to improve the diffraction efficiency of binary pupils [18,19].

Finally, we can study how the on-axis irradiance profile develops when the area of the transparent rings is modified. This is useful for achieving a deep insight into the focusing features of FraGZPs. Here, the period of the binary pupil is fixed and, consequently, so are the inner radii $r_{im}=a[p(m-1)]^{1/2}$. Then, the outer radii are displaced all together in accordance with the expression $r_{om}=a\{p[m-(1-1/\gamma)]\}^{1/2}$, where $\gamma\geq 1$ is a real number. Now, the radius of the outermost transparent ring is no longer a constant but changes with γ as $r_{oM}^2=a^2[1-p(1-\varepsilon/\gamma)/\varepsilon]$. Under these conditions, we can use Eq. (3) for $R=0$ to make animations of the irradiance evolution as the parameter γ increases (or decreases). By so doing, it is possible to see characteristic irradiance shapes when γ takes positive integer values. In particular, those obtained for $\gamma=2$ when $\varepsilon=2$, $\varepsilon=3$, and $\varepsilon=4$ are shown in Figs. 5(a)–5(c), respectively. The corresponding binary pupils are also depicted at the top of Fig. 5. Note that the form of a characteristic profile depends on the particular value of γ, whereas the relative peak heights of their foci will depend on the period p.

4. HIGHLIGHTING PRINCIPAL ATTRIBUTES OF FRACTAL GENERALIZED ZONE PLATES

In comparison with conventional FraZPs, the particular features of the FraGZPs introduced above can be summarized as follows:
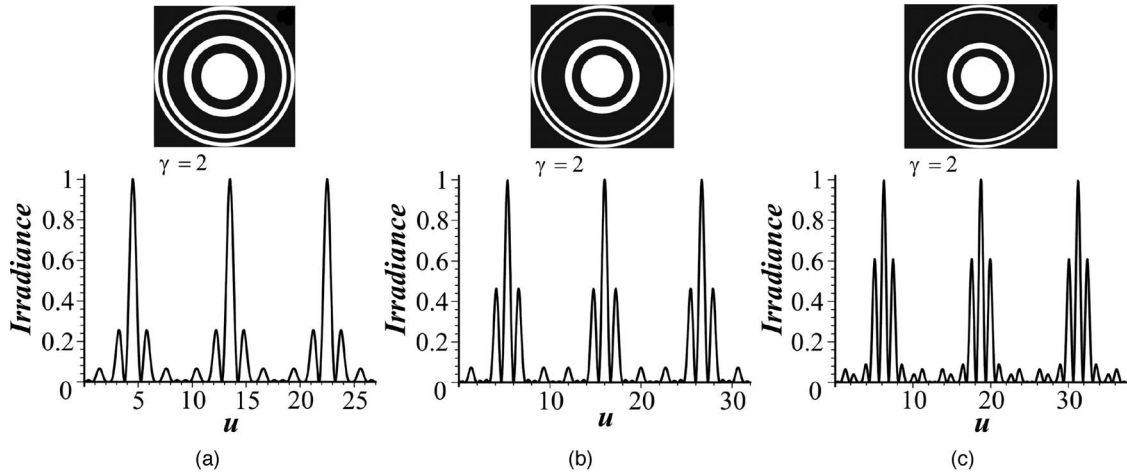
Fig. 5.   Normalized on-axis irradiance of FraGZPs as a function of the normalized variable u with (a) $\varepsilon=2$, (b) $\varepsilon=3$, (c) $\varepsilon=4$. In all cases $N=2$ and $S=2$.

1. In contrast to FraZPs, the ratio between areas of the whole period and its transparent part for FraGZPs can be changed into positive integer numbers $\varepsilon \geqslant 2$. This fact provides a more general procedure for constructing self-similar structures (see Fig. 1). In the particular case of $\varepsilon=2$, our fractal structures reduce to FraZPs, and, consequently, the analytical expression for the on-axis irradiance given by Eq. (1) becomes that of FraZPs.

2. The number of foci within a characteristic irradiance profile is increased by $(\varepsilon-1)(\varepsilon+1)^{S-1}-3^{S-1}$ for an even value of the parameter ε and by $(\varepsilon-1)\varepsilon^{S-1}-2^{S-1}$ for an odd value of ε. The relative peak heights of the most important foci within a characteristic irradiance profile show less discrepancy than those of FraZPs. Therefore, the energy of the diffracted field is redistributed among foci in such a way as to generate a more uniform illumination than in the case of FraZPs. Notice that these features are significant for obtaining high-quality images under polychromatic illumination [9,19].

3. The off-axis irradiance behavior of FraGZPs and FraZPs suggests that they could be used as lenses to enhance the resolving power of a GZP (see Fig. 3). For FraGZPs, this effect can be expected within a multifocal arrangement.

4. The diffraction efficiency along the optical axis of FraGZPs within a characteristic irradiance profile becomes higher as the parameter ε increases. From previous results,

$$E_{FraGZP} - E_{FraZP} = 2N^S[\varepsilon N - (\varepsilon - 1)]^S - 2N^S(2N - 1)^S > 0.$$

Basically, the above-mentioned attributes support the introduction of the fractal structures discussed in this paper as novel diffraction elements. When $\varepsilon \neq 2$, the geometrical shape of these elements and their diffraction behavior clearly differ from those of conventional fractal plates. We believe that, depending on the application in which they are used, FraGZPs can enhance the performance of FraZPs.

5. CONCLUSIONS

In this paper we have presented FraGZPs constructed from periodic diffractive optical elements. The analytical expressions for the on-axis irradiance as well as for the position and height of the principal foci were obtained. The on-axis irradiance curves are related to those of the corresponding GZPs by common foci (see Fig. 2). An approximate analytical expression for the irradiance in the close vicinity of the optical axis was also derived. This allowed the off-axis structure of foci to be analyzed so as to determine, for instance, their transversal width and the energy efficiency of FraGZPs. Finally, we also realize that a similar study for FraGZPs could be carried out with a different approach [20].

REFERENCES

1. H. Takayasu, *Fractals in Physical Science* (Manchester University, 1990).
2. G. Saavedra, W. D. Furlan, and J. A. Monsoriu, "Fractal zone plates," Opt. Lett. **28**, 971–973 (2003).
3. J. A. Monsoriu, G. Saavedra, and W. D. Furlan, "Fractal zone plates with variable lacunarity," Opt. Express **12**, 4227–4234 (2004).
4. G. S. Waldman, "Variations on the Fresnel zone plate," J. Opt. Soc. Am. **56**, 215–218 (1966).
5. M. Bottema, "Fresnel zone-plate diffraction patterns," J. Opt. Soc. Am. **59**, 1632–1638 (1969).
6. J. A. Davis, L. Ramirez, J. A. R. Martín-Romo, T. Alieva, and M. L. Calvo, "Focusing properties of fractal zone plates: experimental implementation with a liquid-crystal display," Opt. Lett. **29**, 1321–1323 (2004).
7. H.-T. Dai, X. Wang, and K.-S. Xu, "Focusing properties of fractal zone plates with variable lacunarity: experimental studies based on liquid crystal on silicon," Chin. Phys. Lett. **22**, 2851–2854 (2005).
8. S. H. Tao, X. C. Yuan, J. Lin, and R. E. Burge, "Sequence of

focused optical vortices generated by a spiral fractal zone plate," Appl. Phys. Lett. **89**, 031105 (2006).

9. W. D. Furlan, G. Saavedra, and J. A. Monsoriu, "White-light imaging with fractal zone plates," Opt. Lett. **32**, 2109–2111 (2007).

10. O. Mendoza-Yero, G. Mínguez-Vega, J. Lancis, and V. Climent, "Focusing and spectral characteristics of periodic diffractive optical elements with circular symmetry under femtosecond pulsed illumination," J. Opt. Soc. Am. A **24**, 3600–3605 (2007).

11. A. Sakdinawat and Y. Liu, "Phase contrast soft x-ray microscopy using Zernike zone plates," Opt. Express **16**, 1559–1564 (2008).

12. S. Wang and X.-C. Zhang, "Tomographic imaging with a terahertz binary lens," Appl. Phys. Lett. **82**, 1821–1823 (2003).

13. O. Mendoza-Yero, G. Mínguez-Vega, J. Lancis, E. Tajahuerce, and V. Climent, "Spectral analysis of femtosecond pulse diffraction through binary diffractive optical elements: theory and experiment," Opt. Express **16**, 2541–2546 (2008).

14. K. Shi, S. Yin, and Z. Liu, "Wavelength division scanning for two-photon excitation fluorescence imaging," J. Microsc. **223**, 83–87 (2006).

15. R. Zheng, L. Jiang, and M. Feldman, "Properties of zone plates used for lithography," J. Vac. Sci. Technol. B **24**, 2844–2847 (2006).

16. S. Cavalieri, L. Fini, E. Sali, and R. Buffa, "Enhancement of harmonic generation by Fresnel-lensing effects," Opt. Lett. **31**, 1298–1300 (2006).

17. X. Ni, C. Wang, X. Liang, M. Alrubaiee, and R. R. Alfano, "Fresnel diffraction supercontinuum generation," IEEE J. Sel. Top. Quantum Electron. **10**, 1229–1231 (2004).

18. J. A. Monsoriu, W. D. Furlan, G. Saavedra, and F. Giménez, "Devil's lenses," Opt. Express **15**, 13858–13864 (2007).

19. W. Dong, N. Li-Gang, C. Qi-Dai, W. Rui, and S. Hong-Bo, "High efficiency multilevel phase-type fractal zone plates," Opt. Lett. **33**, 2913–2915 (2008).

20. J. A. Davis, S. P. Sigarlaki, J. M. Craven, and M. L. Calvo, "Fourier series analysis of fractal lenses: theory and experiments with a liquid-crystal display," Appl. Opt. **45**, 1187–1192 (2006).